Ionics (2015) 21:1427–1434
DOI 10.1007/s11581-014-1310-1

ORIGINAL PAPER

Highly enhanced electrochemical responses of rutin by nanostructured Fe_2O_3/RGO composites

Yan Wu · Chenxi Hu · Meng Huang · Nannan Song · Weibing Hu

Received: 30 May 2014 / Revised: 14 October 2014 / Accepted: 9 November 2014 / Published online: 21 November 2014

Abstract Fe_2O_3/reduced graphene oxide (RGO) nanocomposites were prepared by a hydrothermal reduction using $Fe(OH)_3$ and graphene oxide (GO) precursors, which were assembled electrostatically by mixing a negatively charged GO aqueous suspension with a positively charged $Fe(OH)_3$ solution at room temperature. The resulting composites were characterized using XRD, SEM, FTIR, and TGA, and then were used to modify the glassy carbon electrode (GCE). The electrochemical behavior of rutin on different types of electrode was compared, and the Fe_2O_3/RGO composite enhanced electrochemical catalysis effect on rutin, and suitable for rutin detection with high sensitivity and short response time. After 90 s, under open circuit potential, the linear range was increased from 1.5×10^{-8} to 1.8×10^{-5} M, and the detection limit was reduced to 9.8×10^{-9} M. This method of analysis has high recovery ratio of rutin up to 99.5 %.

Keywords Composite materials · Nanostructures · Chemical synthesis · Electrochemical properties

Introduction

Rutin, 3′,4′,5,7-tetrahydroxyflavone-3β-D-rutinoside, is one of the most abundant flavonoids which are a group of antioxidizing active polyphenolic compounds [1, 2]. It shows that rutin acts as a scavenger of various oxidizing species, i.e., superoxide anion, hydroxyl radical, and peroxyl radicals [3], and has been widely used clinically as the therapeutical medicines [4]. Therefore, it is quite important and interesting to develop simple and sensitive methods to determine rutin. Recently, some techniques have been established for this purpose, such as the high-performance liquid chromatography (HPLC) [5], sequential injection analysis [6], electrochemiluminescence [7], capillary zone electrophoresis [8], reversed-phase liquid chromatography (RPLC) [9], flow injection analysis [10], chemiluminescence [11], spectrophotometry [12], and electrochemistry methods [13]. Among these techniques, the electroanalytical technique exhibits many advantages, such as convenient handling, low cost, short analysis time, and high sensitivity.

Graphene, a 2D monolayer of sp^2 carbon in a honeycomb-like network [14], has attracted infinite scientific interest due to its outstanding optical, thermal, electrical, and mechanical properties [15]. Graphene-based composites with the advanced properties of graphene, such as graphene-transition metal oxide composites and graphene-conducting composites, have large surface areas and good electrical conductivities, and have been investigated for electrochemical sensors [16, 17], either as electrode materials [18, 19] or as platforms for metal oxide nanoparticles to avoid their agglomeration [20]. Recently, graphene, a rising star in the carbon family, has been proposed as an ideal matrix for various composites used in detection of rutin because of its excellent electronic properties, superior chemical stability, and high specific surface area [21–25]. For instance, Yang et al. incorporated Ag nanoparticles into poly(methylene blue) functionalized graphene to

---

Electronic supplementary material The online version of this article (doi:10.1007/s11581-014-1310-1) contains supplementary material, which is available to authorized users.

Y. Wu · N. Song · W. Hu (✉)
Key Laboratory of Biological Resources Protection and Utilization of Hubei Province, Hubei University for Nationalities,
Enshi 445000, China
e-mail: chemistryhu@126.com

C. Hu
School of Materials Science and Engineering, Shandong University,
Jinan 250061, China

Y. Wu · M. Huang · W. Hu
School of Chemical and Environmental Engineering,
Hubei University for Nationalities, Enshi 445000, China

Scheme 1 The preparation course of the Fe_2O_3/RGO nanocomposites

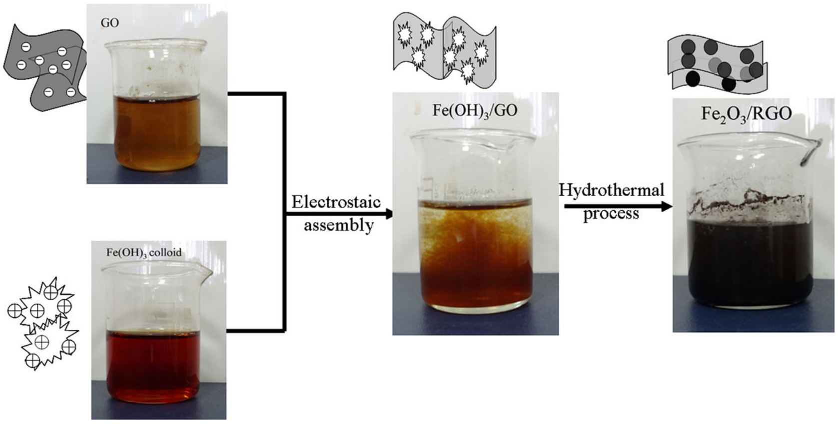

prepare a Ag nanoparticles/poly(methylene blue) functionalized graphene nanocomposite (AgNPs/PMB–GR) film modified electrode for sensitive determination of rutin. The results demonstrated that the AgNPs/PMB–GR could remarkably increase the redox currents of rutin, and the lowest detectable concentration was 1×10^{-8} M [21]. A similar effect of MnO_2 incorporation has also been demonstrated in MnO_2–graphene composites [22]. However, to the best of our knowledge, electrochemical determination of rutin using electrode modified by the Fe_2O_3/RGO composite has not been reported. In this study, we developed a facile electrostatic-assisted self-assembly method for the preparation of Fe_2O_3/RGO nanocomposites from $Fe(OH)_3$/graphene oxide (GO). The Fe_2O_3/RGO nanocomposites will be used to modify different glassy carbon electrodes (GCEs) for rutin detection.

Experimental

Synthesis of Fe_2O_3 nanoparticles, RGO, and Fe_2O_3/RGO composites

In a typical procedure, a 100 mL of 0.1 M $FeCl_3$ aqueous solution in a beaker was boiled to form a stable $Fe(OH)_3$ colloidal suspension of positively charged.

Fifty-milligram GO, synthesized by a modified Hummer's method [17], was ultrasonically dispersed in 50 mL H_2O for 1.5 h to acquire a stable GO suspension. The pH of the suspension was adjusted close to 6.2 with a zeta potential of −42 mV using 1 M NaOH and 1 M HCl solutions [26]. At this pH, the GO nanosheets were negatively charged. Then, the above GO suspension was quickly mixed with the $Fe(OH)_3$ solution under vigorous stirring. Since the $Fe(OH)_3$ molecules were positively charged, they quickly assembled with the negatively charged GO and formed a flocculent suspension within a few minutes. Finally, the mixed flocculent suspension was transferred to a 100-mL Teflon container. After sealing, the Teflon-lined stainless steel pressure vessel was heated at 180 °C for 12 h. With the same method, Fe_2O_3 nanoparticles [27] were also obtained without using the negatively charged GO, and RGO [28] was obtained without involving the $Fe(OH)_3$ colloidal solution, for comparison. After the reaction, the product was centrifuged and washed with distilled water and acetone, for three times, then dried at 60 °C. The synthetic process is shown in Scheme 1.

The modification of GCEs

Fe_2O_3 nanoparticles, RGOs, and Fe_2O_3/RGO composites (10.0 mg each) were respectively added into 10 mL of cyclohexanol, and sonically treated using a KQ3200DE ultrasonicator for 1 h. Before modification, the GCEs with a diameter of 3 mm were polished with 0.05-mm alumina paste, and then sonicated in double-distilled water for 2 min. The GCEs were then coated with 10 μL Fe_2O_3, RGO, and Fe_2O_3/RGO suspension. After the evaporation of the cyclohexanol under an infrared lamp in air, the modified GCEs (Fe_2O_3/GCEs, RGO/GCEs and Fe_2O_3/RGO/GCEs) were obtained.

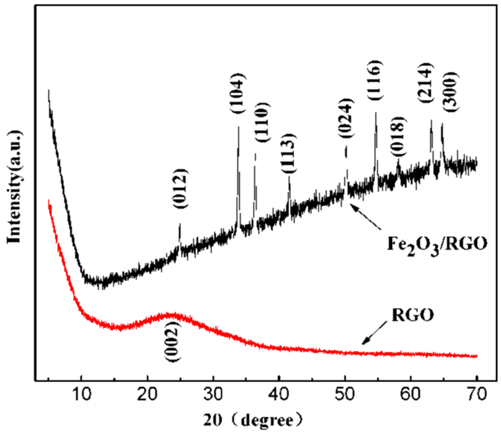

Fig. 1 XRD patterns of RGO and Fe_2O_3/RGO

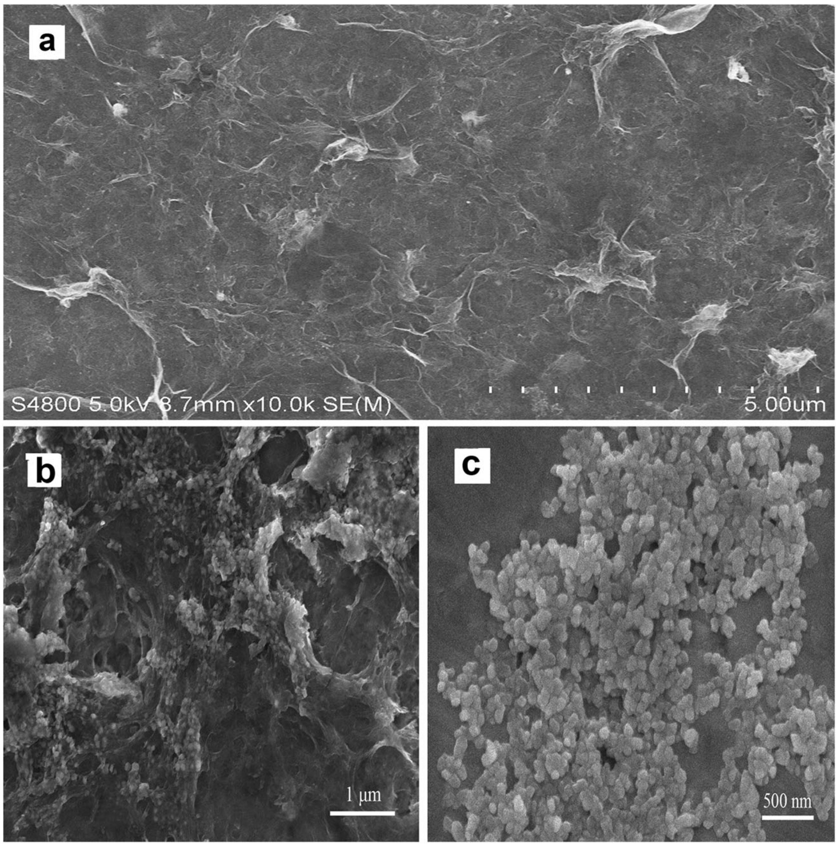

Fig. 2 SEM images of RGO, Fe_2O_3/RGO, and Fe_2O_3

Characterization

The morphology of the materials was tested by using a SEM (JSM-6510LV, Japan). The structure of products was characterized by X-ray diffraction (XRD) (Shimadzu XRD-7000, Japan) using Cu-Ka radiation (γ for Kα=1.54 Å) at 40 kV and 40 mA. Infrared spectra of products were recorded on a Nicolet 360 Fourier transform infrared (FTIR) instrument using KBr pellet in the 400~4000 cm^{-1} range. Thermogravimetric analysis (TGA) was conducted on a DSCQ1000 instrument from 50 to 1000 °C at a heating rate of 10 °C min^{-1} in air.

All the electrochemical measurements were carried out using a 660D electrochemical analyzer (CH Instruments, USA). A conventional three-electrode system, consisting of Fe_2O_3/RGO composite modified working GCE, a saturated calomel reference electrode (SCE), and a platinum wire auxiliary electrode, was employed. A 0.1 M and pH 5.7 phosphate-buffered saline (PBS) solution was used as the supporting electrolyte for the detection of rutin. The cyclic voltammetry (CV) tests were conducted at a scan rate of 0.1 V s^{-1} from 0 to 0.8 V. Differential pulse voltammetry

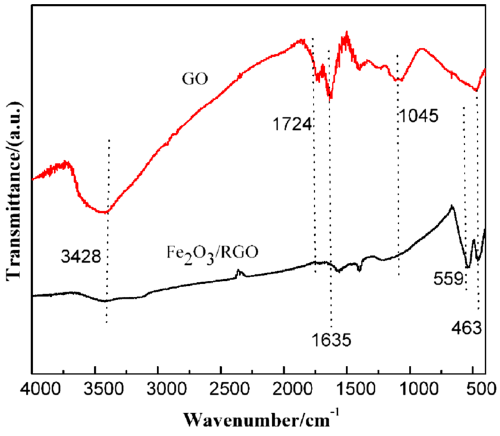

Fig. 3 FTIR spectra of GO and Fe_2O_3/RGO composites

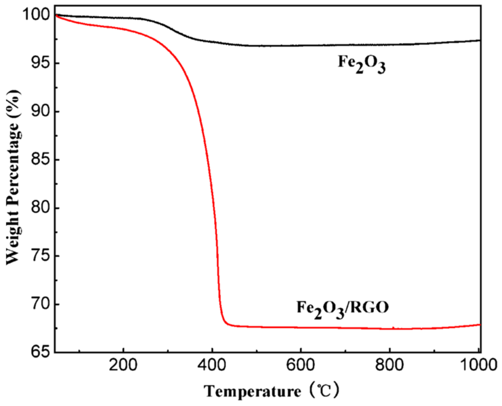

Fig. 4 TGA curves of Fe_2O_3 and Fe_2O_3/RGO

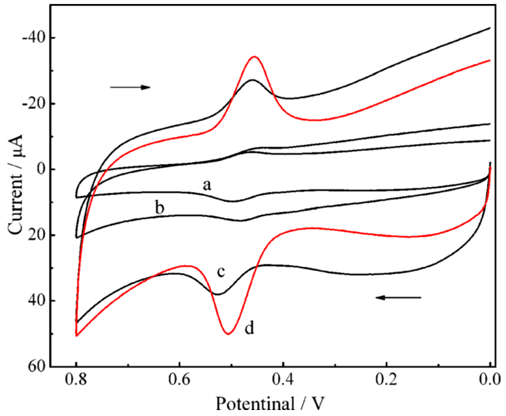

Fig. 5 CV curves of 2 μM rutin on GCE (**a**), Fe_2O_3/GCE (**b**), RGO/GCE (**c**), and Fe_2O_3/RGO/GCE (**d**) in pH 5.7 PBS solution

(DPV) was used to study the electrochemical behavior in low rutin concentrations from 0.1 to 0.8 V.

Results and discussion

Morphology and structures

Figure 1 shows the XRD patterns of the RGO and Fe_2O_3/RGO composites. The dominant diffraction peaks can be attributed to Fe_2O_3 for Fe_2O_3/RGO (JCPDS No. 33-0664). A wide peak of RGO appears in the range of 24°–26°, which is consistent with Shin et al. [29]. Compared with the peaks of the Fe_2O_3/RGO nanocomposites, the small diffraction peaks of the RGO indicate that the RGO nanosheets were sufficiently exfoliated by the attached Fe_2O_3 nanoparticles [30]. These results show that the as-acquired composites consist of disorderedly stacked graphene and well-crystallized Fe_2O_3 nanoparticles.

The SEM observation results of the materials are presented in Fig. 2. As shown in Fig. 2a, the RGO film demonstrated a curly and corrugated appearance consisting of a wrinkled paper-like structure. Figure 2b clearly shows that the Fe_2O_3 nanoparticles are uniformly confined between the RGO nanosheets. Even though undergone strong sonications, the nanoparticles were still firmly attached onto the RGO nanosheets, which implies a vigorous interaction between the Fe_2O_3 and the RGO. Without such confinements by the RGO, Fe_2O_3 nanoparticles tend to be collective as shown in Fig. 2c. Figure 2b, c reveals that the average diameter of the Fe_2O_3 nanoparticles is about 110 nm.

FTIR spectroscopy was employed to measure the structural change in bonding related to the GO and Fe_2O_3/RGO composites, and the results are shown in Fig. 3. The broad absorptions at about 3428 and 1635 cm^{-1} are assigned to the hydroxyl groups. The absorption band at 1045 cm^{-1} can be assigned to the stretching vibration of C–O. The C=O vibration band at 1724 cm^{-1} (for Fe_2O_3/RGO) is much weaker after the hydrothermal reaction, due to the transition of GO to RGO [31, 32]. In addition, the strong absorption bands at 559 and 463 cm^{-1} are attributed to the vibration of the Fe–O bond [33].

Figure 4 shows the TGA profiles of both the Fe_2O_3/RGO and the bare Fe_2O_3 nanoparticles, from room temperature to 1000 °C in air. The small weight loss of Fe_2O_3 below 350 °C is due to the evaporation of moisture or gaseous absorbed in the nanocomposites [34]. For the Fe_2O_3/RGO, there is a small stage of weight loss below 350 °C, which could be ascribed to the reduced hydroxyl groups in the RGO and possible water absorbed during the IR measurements [35]. However, the weight loss from 350–430 °C is due to the combustion of carbon in air. This is confirmed by the TGA curve of the bare RGO in the same temperature range. Thus, according to the above analysis, the carbon content in the Fe_2O_3/RGO nanocomposites is ~67.57 wt%.

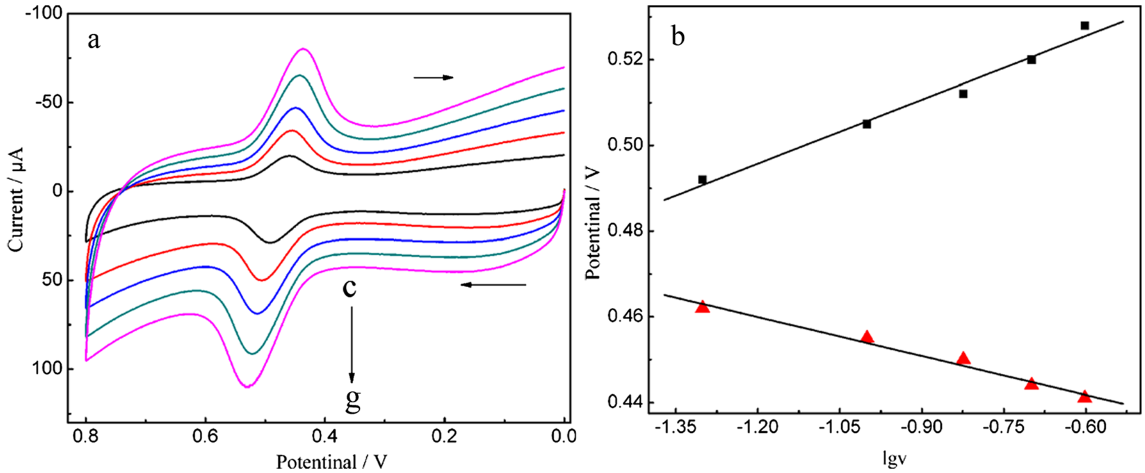

Fig. 6 **a** Cyclic voltammograms of 2 μM rutin with different scan rate (υ) for Fe_2O_3/RGO/GCE in pH 5.7 PBS (**c**–**g** 0.05, 0.1, 0.15, 0.2, and 0.25 V s^{-1}, respectively); **b** linear relationship between peak potentials (E_p) and lgυ

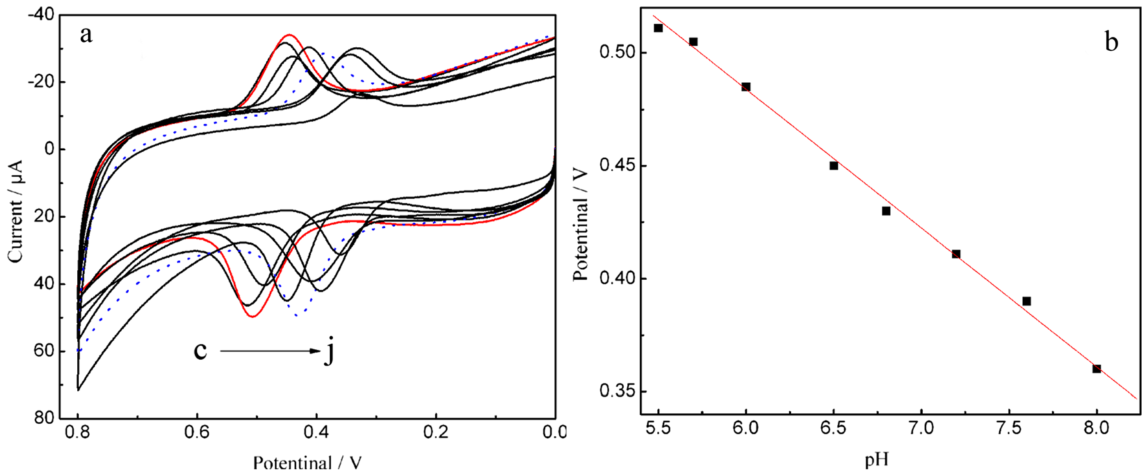

Fig. 7 **a** Cyclic voltammograms of 2 μM rutin on Fe_2O_3/RGO/GCE with different pH PBS (**c**–**j** 5.5, 5.7, 6.0, 6.5, 6.8, 7.2, 7.6, and 8.0, respectively), scan rate 0.1 V s^{-1}; **b** the relationship between the formal potential (E_{pa}) and pH

Rutin detection

The electrochemical responses of rutin on the surface of GCE, Fe_2O_3, RGO, and Fe_2O_3/RGO modified GCEs were studied by using a CV. Figure 5 shows the CV curves of 2 μM rutin in a pH 5.7 PBS solution. No redox peak was noticed for the GCE, Fe_2O_3/GCE, RGO/GCE, and Fe_2O_3/RGO/GCE in a blank PBS solution, indicating that all the modified materials were electrochemically inactive in the selected potential range. As can be seen in Fig. 5, a pair of small redox peaks were found at the bare GCE in the potential scan from 0 to 0.8 V when rutin was added into the buffer solution (curve a), which can be attributed to the redox behavior of rutin at the GCE surface. The small redox peak showed a weak oxidation process, resulting from the weak adsorption and the slow electron transfer rates at the GCE surface. For Fe_2O_3/GCE (curve b), the redox peak current of rutin increased and the background current of Fe_2O_3/GCE increased obviously, due to that the presence of the Fe_2O_3 increased the capacitance currents. The redox peak current of rutin increased further at RGO/GCE (curve d). This should be attributed to the effective accumulation and promotion effect of the RGO, as described in previous reports [36, 37]. The accumulation made more rutin involved the electrochemical reaction and increased the electron-transfer rates between rutin and the electrode. Furthermore, the electrochemical behavior of rutin showed a great difference on the surface of Fe_2O_3/RGO/GCE (curve e). First, the redox peak currents were much higher than that of above electrodes and the ratio of the redox peak current (I_{pa}/I_{pc}) was 1.32. Second, the peak potential separation decreased to 39 mV, which is lower than that of a single material modified GCEs. According to Nicholson's theory [38, 39], a smaller peak potential separation reveals a better reversibility and a higher heterogeneous electron exchange rate. The improved performance of the Fe_2O_3/RGO composite should be attributed to the synergistic effect of Fe_2O_3 and RGO: (i) In the composite, RGO sheets act as a conductive support, on which Fe_2O_3 nanoparticles are uniformly

Fig. 8 Electrochemical reaction mechanism of rutin

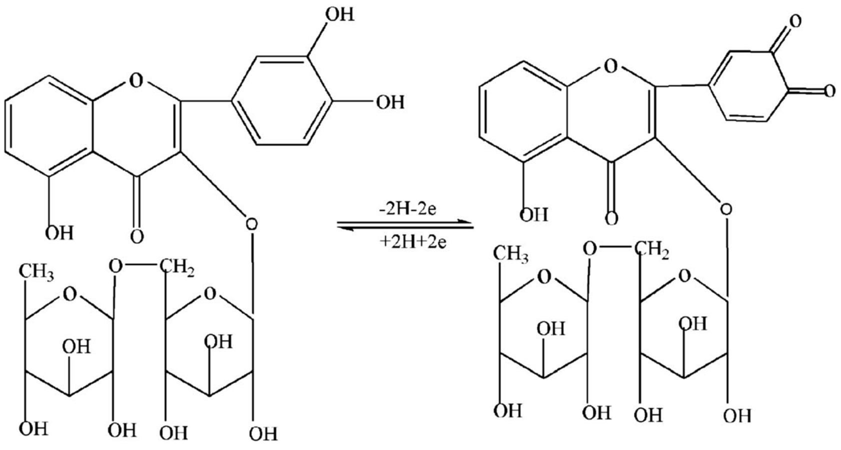

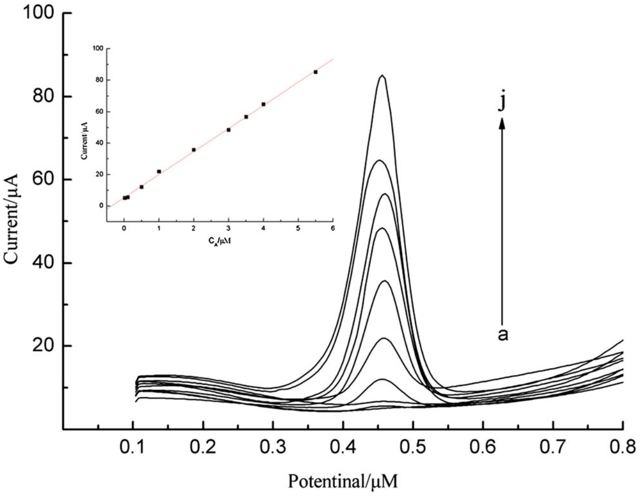

Fig. 9 DPV curves of rutin at different concentration (**a**–**j**): 0, 0.02, 0.1, 0.5, 1, 2, 3, 3.5, 4, and 5.5 μM; *inset* shows the relationship of the anodic peak currents versus rutin concentration

anchored, and this ensures the electrochemical activity of the Fe_2O_3 nanoparticles because of good electron transfer; (ii) RGO sheets serve as 2D conductively connecting the Fe_2O_3 nanoparticles decorated RGO sheets, forming a 3D conductive network. The excellent conductivity and the large specific surface areas of the Fe_2O_3/RGO composite exhibited a strong adsorptive ability and provided numerous active sites for rutin. The synergistic effect between the Fe_2O_3 nanoparticles and the RGO nanosheets can effectively promote the electron transmission. Hence, to achieve high sensitivity and good reproducibility, the Fe_2O_3/RGO/GCE was chosen for the analysis of rutin, and the oxidation peak was considered as standard because it is higher than the reduction peak (I_{pa}/I_{pc}=1.32).

Effects of scan rate and pH value

In order to further investigate the characteristics of rutin at the Fe_2O_3/RGO/GCE surface, the effect of scan rate on the redox behavior of 2 μM rutin was investigated in the 0.1 M pH 5.7 PBS solution using a CV. The redox peak current increased gradually with the increase of scan rates in the range from 0.05 to 0.25 V s^{-1}, along with the changes of the redox peak potentials (Fig. 6). This phenomenon suggests a quasi-reversible electrochemical process. The redox peak potential and lgυ exhibited a good linear relationship with the regression equations, $E_{pa}=0.55538+0.04969\lg\upsilon$ (R=0.9903) and $E_{pc}=0.42359-0.03929\lg\upsilon$ (R=0.9908). According to Laviron theory [40], when the values of ΔE_p are larger than 200/nmV, a graph of $E_p=E_0-(RT/\alpha nF)\ln(\alpha nF/RTk_s)-(RT/\alpha nF)\ln\upsilon$ yields two straight lines with a slope equal to $-2.3RT/\alpha nF$ for the cathodic peak and $2.3RT/(1-\alpha)nF$ for the anodic peak, in which α is the electron transfer coefficient, n is the electron-transfer number, k_s is the rate constant of the reaction, υ is the scan rate, and E_0 is the formal redox potential. Here, we take R=8.314, T=298, and F=96500. So the value of α and n can be easily calculated from $0.04969=2.3RT/(1-\alpha)nF$ and $0.03929=2.3RT/\alpha nF$. Therefore, the charge transfer coefficient α is calculated to be 0.55 and the electron transfer number n is estimated to be 2.3, implying that there are two electrons involved in the oxidation process, which is in accordance with previous report [13]. In addition, with the increase of scan rate, the oxidation (I_{pa}) peak currents of rutin increased gradually and linearly. The linear regression equations can be expressed as $I_{pa}(\mu A)=6.185+187.5\upsilon$ (V s^{-1}) (R=0.9997), indicating that the redox behavior of rutin on Fe_2O_3/RGO/GCE is a typical adsorption-controlled process.

The effect of pH value of the solution on the redox response of 2 μM rutin is shown in Fig. 7. The redox current peaked at the pH 5.7, with the solution pH ranging from 5.5 to 8.0; thus, pH 5.7 was chosen in the following investigation for sensitivities. From Fig. 7a, b, it can also be seen that the redox peak potentials shifted negatively and linearly when the pH values increased from 5.5 to 8.0. The linear regression equation of the oxidation peak can be expressed as E_{pa}=0.85293−0.0615 pH (R=0.9981). The slope value of 61.5 mV pH^{-1} was close to the theoretical value of 59 mV pH^{-1}, indicating that the same amounts of electrons and protons took part in the electrode reaction [41], namely two electrons and two protons were involved in the reaction. The redox mechanism of for rutin at the Fe_2O_3/RGO/GCE is illustrated in Fig. 8.

Electrochemical detection of rutin

Accumulation time can effectively increase the adsorption of rutin on the electrode surface, thereby enhancing the redox response and improving the detection sensitivity. The oxidation peak current increased gradually with increasing accumulation time to 90 s and only increased slightly when the time exceeded 90 s. Therefore, 90 s was

Table 1 Determination recovery of rutin

Found before adding (M)	Added (M)	Found after adding (M)	Recovery (%)	RSD (%), n=5
5.0×10^{-7}	0	4.7×10^{-7}	94.0	2.7
	5.0×10^{-7}	9.6×10^{-7}	96.0	4.2
	1.0×10^{-6}	2.1×10^{-6}	105.0	2.7

Table 2 Determination of rutin in drug tablets by DPV ($n=5$)

Sample	Specified (mg/tablet)	Detected (mg/tablet)	RSD (%)	Added (mg/L)	Found (mg/L)	Average recovery (%)
1	20	19.3	2.06	0.75	0.723	96.4
2	20	19.6	0.85	0.75	0.738	98.4
3	20	20.2	1.27	0.75	0.759	101.2

chosen as the accumulation time. To investigate the effect of accumulation potentials on the redox behavior of rutin, we shifted the potentials from −0.2 to 0.3 V at a fixed accumulation time of 90 s and only found out a slight peak current change. Therefore, the accumulation potential has no obvious impact on the oxidation peak current. The accumulation was employed under open circuit.

The Fe_2O_3/RGO modified GCE was used for the single measurement in this work. The reproducibility for multiple modified GCEs was estimated by measuring the peak current of 1 μM rutin. In order to obtain good reproducibility, each freshly modified electrode needs to be swept in the PBS solution until background current minimized and stabilized. The relative standard deviation (RSD) is 2.8 % for eight Fe_2O_3/RGO modified GCEs, indicative of a good reproducibility.

Under the optimal conditions, a differential pulse voltammetry (DPV) was used to determine the rutin due to its high sensitivity and selectivity (Fig. 9). Figure S1 shows the DPV curves of the lower concentration addition of rutin. In the inset of Fig. 9, the oxidation peak current of rutin (I_A, μA) was linear with its concentration (C_A, μM) over the range of 1.5×10^{-8}~1.8×10^{-5} M, obeying the following equation: I_{pa} (μA)=14.3696 C_A (μM)−0.0887. The correlation coefficient was 0.9989, suggesting a good linearity. After 90-s accumulation under open circuit potential, the limit of detection was evaluated to be 9.8×10^{-9} M, based on three signal to noise ratios. The comparison of Fe_2O_3/RGO/GCE with other modified electrodes for rutin determination is listed in Table S1.

The potential interferences of some foreign species on the determination of rutin were also examined. There was no influence on the determination of 1 μM rutin when 500-fold concentration of common ions (Cu^{2+}, Fe^{3+}, Mg^{2+}, Zn^{2+}, Pb^{2+}) or 100-fold of the pyrogallol, resorcinol, and 2-nitrophenol were added to the electrolytic cell, indicating a high selectivity.

Under the optimized conditions, rutin in a mixed solution of ethanol and PBS was determined using a standard addition method, and each concentration was continuously measured for five times. Table 1 shows the results of recycling experiments. These results show clearly that the recovery was between 94.0 and 105.0 %. The correlation coefficient was under 5 %.

Real samples analysis

The dosage forms of rutin, tablets, declared content of 20 mg rutin per each unit, were bought from Shanxi Yunpeng Pharmaceutical Co. Ltd., China. To further validate out technique for the detection of rutin, drug tablet was dissolved in ethanol, the ethanol solution of drug tablet for the detection was accurately diluted with a PBS. The determination of rutin was conducted by the proposed method. As shown in Table 2, the results obtained by the proposed method are in good agreement with label amount. From Table 2, the recovery of five independent experiments varied from 96.4 to 101.2 %, and the content of rutin is calculated to be 19.89 mg per tablet, demonstrating the accuracy of the proposed method. The experimental results demonstrated that the proposed methods could be efficiently used for the determination of rutin.

Conclusion

In summary, the Fe_2O_3/RGO nanocomposites were prepared by a facile method in aqueous solution, with an electrostatic interaction assisted assembly followed by a hydrothermal process. The glassy carbon electrodes modified by the resulting Fe_2O_3/RGO nanocomposites have been successfully used to measure the rutin contents by an electrochemical method. The synergistic effect between the Fe_2O_3 nanoparticles and the RGO nanosheets resulted in efficient transports of electrons and ions, which lead to significantly improved current values of the oxidation peaks for rutin. The use of the Fe_2O_3/RGO modified electrodes can reliably and effectively determine low rutin concentrations, with a detection limitation as low as 9.8×10^{-9} M.

Acknowledgments The work was funded by the National Natural Science Foundation of China (21461008), Open Foundation of Key Laboratory of Biologic Resources Protection and Utilization of Hubei Province, Forestry Key Discipline (PKLHB1303), and Hubei University for Nationalities (MY2009B007).

References

1. Dias K, Nikolaou S, Giovani WFD (2008) Synthesis and spectral investigation of Al(III) catechin/β-cyclodextrin and Al(III) quercetin/

β-cyclodextrin inclusion compounds. Spectrochim Acta A Mol Biomol Spectrosc 70:154–161

2. He JB, Wang Y, Deng N, Lin XQ (2007) Study of the adsorption and oxidation of antioxidant rutin by cyclic voltammetry-voltabsorptometry. Bioelectrochemistry 71:157–163
3. Zhang Y, Zheng JB (2008) Sensitive voltammetric determination of rutin at an ionic liquid modified carbon paste electrode. Talanta 77: 325–330
4. Wu SH, Sun JJ, Zhang DF, Lin ZB, Nie FH, Qiu HY, Chen GN (2008) Nanomolar detection of rutin based on adsorptive stripping analysis at single-sided heated graphite cylindrical electrodes with direct current heating. Electrochim Acta 53:6596–6601
5. Kazuo I, Takashi F, Yasuji K (2001) Determination of rutin in human plasma by high-performance liquid chromatography utilizing solid-phase extraction and ultraviolet detection. J Chromatogr B Biomed Sci Appl 759:161–168
6. Legnerová Z, Šatínský D, Solich P (2003) Using on-line solid phase extraction for simultaneous determination of ascorbic acid and rutin trihydrate by sequential injection analysis. Anal Chim Acta 497:165–174
7. Liang YD, Song JJ (2008) Electrochemiluminescence from direct electro-oxidations of organic analyte rutin and its analytical application. J Electroanal Chem 624:27–32
8. Wang QJ, Ding F, Li H, He PG, Fang YZ (2003) Determination of hydrochlorothiazide and rutin in Chinese herb medicines and human urine by capillary zone electrophoresis with amperometric detection. J Pharm Biomed Anal 30:1507–1514
9. Pilar V, Carmen LE, Juan MH, Manul HC (2000) Determination of phenols in wines by liquid chromatography with photodiode array and fluorescence detection. J Chromatogr A 871:85–93
10. He CX, Cui H, Zhao XY, Zhao HZ, Zhao GW (1999) Determination of rutin by flow injection with inhibited chemiluminescence detection. Anal Lett 32:2751–2759
11. Song ZH, Hou S (2002) Sensitive determination of sub-nanogram amounts of rutin by its inhibition on chemiluminescence with immobilized reagents. Talanta 57:59–67
12. Hassan HNA, Barsoum BN, Habib IHI (1999) Simultaneous spectrophotometric determination of rutin, quercetin and ascorbic acid in drugs using a Kalman Filter approach. J Pharm Biomed Anal 20: 315–320
13. Sun W, Yang MX, Li YZ, Jiang Q, Liu SF, Jiao K (2008) Electrochemical behavior and determination of rutin on a pyridinium-based ionic liquid modified carbon paste electrode. J Pharm Biomed Anal 48:1326–1331
14. Geim AK, Novoselov KS (2007) The rise of grapheme. Nat Mater 6: 183–191
15. Novoselov KS, Geim AK, Morozov SV, Jiang D, Katsnelson MI, Grigorieva IV, Dubonos SV, Firsov AA (2005) Tow-dimensional gas of massless Dirac fermions in grapheme. Nature 438:197–200
16. Yin HS, Zhou YL, Ma Q, Ai SY, Chen QP, Zhu LS (2010) Electrocatalytic oxidation behavior of guanosine at graphene, chitosan and Fe_3O_4 nanoparticles modified glassy carbon electrode and its determination. Talanta 82:1993–1199
17. Huang M, Wu Y, Hu WB (2014) A facile synthesis of reduced graphene oxide-wrapped WO_3 nanowire composite and its enhanced electrochemical catalysis properties. Ceram Int 40:7219–7225
18. Wang C, Zhang L, Guo ZH, Xu JG, Wang HY, Zhai KF, Zhuo X (2010) A novel hydrazine electrochemical sensor based on the high specific surface area graphene. Microchim Acta 169:1–6
19. Kuila T, Bose S, Khanra P, Mishra AK, Kim NH, Lee JH (2011) Recent advances in graphene-based biosensors. Biosens Bioelectron 26:4637–4648
20. Xiang CC, Li M, Zhi MJ, Manivannanc A, Wu NQ (2012) Reduced graphene oxide/titanium dioxide composites for supercapacitor electrodes: shape and coupling effects. J Mater Chem 22:19161–19167
21. Yang SL, Li G, Zhao JH, Zhu HM, Qu LB (2014) Electrochemical preparation of Ag nanoparticles/poly(methylene blue) functionalized graphene nanocomposite film modified electrode for sensitive determination of rutin. J Electroanal Chem 717–718:225–230
22. Sun W, Wang XZ, Zhu HH, Sun XH, Shi F, Li GN, Sun ZF (2013) Graphene-MnO_2 nanocomposite modified carbon ionic liquid electrode for the sensitive electrochemical detection of rutin. Sensors Actuators B Chem 178:443–449
23. An J, Bi YY, Yang CX, Hu FD, Wang CM (2013) Electrochemical study and application on rutin at chitosan/graphene films modified glassy carbon electrode. J Pharm Anal 3:102–108
24. Sun W, Wang D, Zhang YY, Ju XM, Yang HX, Chen YX, Sun ZF (2013) Electrodeposited graphene and gold nanoparticle modified carbon ionic liquid electrode for sensitive detection of rutin. Chin J Anal Chem 41:709–713
25. Liu KP, Wei JP, Wang CM (2011) Sensitive detection of rutin based on β-cyclodextrin@chemically reduced graphene/Nafion composite film. Electrochim Acta 56:5189–5194
26. Liu Y, Ying YL, Mao YY, Gu L, Wang YW, Peng XS (2013) CuO nanosheets/rGO hybrid lamellar films with enhanced capacitance. Nanoscale 5:9134–9140
27. Wang DW, Li YQ, Wang QH, Wang TM (2012) Nanostructured Fe_2O_3–graphene composite as a novel electrode material for supercapacitors. J Solid State Electrochem 16:2095–2102
28. Nethravathi C, Rajamathi M (2008) Chemically modified graphene sheets produced by the solvothermal reduction of colloidal dispersions of graphite oxide. Carbon 46:1994–1998
29. Shin HJ, Kim KK, Benayad A, Yoon SM, Park HK, Jung IS, Jin MH, Jeong HK, Kim JM, Choi JY, Lee YH (2009) Efficient reduction of graphite oxide by sodium borohydride and its effect on electrical conductance. Adv Funct Mater 19:1987–1992
30. Liu SY, Xie J, Pan Q, Wu CY, Cao GS, Zhu TJ, Zhao XB (2012) Graphene anchored with nanocrystal Fe_2O_3 with improved electrochemical li-storage properties. Int J Electrochem Sci 7:354–362
31. Liu Y, Hu Y, Zhou MJ, Qian HS, Hu X (2012) Microwave-assisted non-aqueous route to deposit well-dispersed ZnO nanocrystals on reduced graphene oxide sheets with improved photoactivity for the decolorization of dyes under visible light. Appl Catal B Environ 125:425–431
32. Zhao YC, Song XY, Song QS, Yin ZL (2012) A facile route to the synthesis copper oxide/reduced graphene oxide nanocomposites and electrochemical detection of catechol organic pollutant. Cryst Eng Commun 14:6710–6719
33. Yariv S, Mendelovici E (1979) The effect of degree of crystallinity on the infrared spectrum of hematite. Appl Spectrosc 33:410–411
34. Chen JS, Tan YL, Li CM, Cheah YL, Luan DY, Madhavi S, Boey FYC, Archer LA, Lou XW (2010) Constructing hierarchical spheres from large ultrathin anatase TiO_2 nanosheets with nearly 100% exposed (001) facets for fast reversible lithium storage. J Am Chem Soc 132:6124–6130
35. Li BJ, Cao HQ, Shao J, Qu MZ, Warner JH (2011) Superparamagnetic Fe_3O_4 nanocrystals@graphene composites for energy storage devices. J Mater Chem 21:5069–5075
36. Li J, Guo SJ, Zhai YM, Wang EK (2009) Nafion-graphene nanocomposite film as enhanced sensing platform for ultrasensitive determination of cadmium. Electrochem Commun 11:1085–1088
37. Kang XH, Wang J, Wu H, Liu J, Aksay IA, Lin YH (2010) A graphene-based electrochemical sensor for sensitive detection of paracetamol. Talanta 81:754–759
38. Nicholson RS, Shain I (1964) Theory of stationary electrode polarography single scan and cyclic methods applied to reversible, irreversible, and kinetic systems. Anal Chem 36:706–723
39. Nicholson RS (1965) Theory and application of cyclic voltammetry for measurement of electrode reaction kinetics. Anal Chem 37:1351–1355
40. Laviron E (1979) General expression of the linear potential sweep voltammogram in the case of diffusionless electrochemical systems. J Electroanal Chem Interfacial Electrochem 101:19–28
41. Bard AJ, Faulkner LR (2001) Electrochemical methods: fundamentals and applications, 2nd edn. Wiley, New York, pp 1–864